

Superconductivity and physical properties of $\text{Ba}_{24}\text{Si}_{100}$ determined from electric transport, specific-heat capacity, and magnetic susceptibility measurements

Takeshi Rachi,¹ Harukazu Yoshino,² Ryotaro Kumashiro,¹ Masaki Kitajima,² Kensuke Kobayashi,² Keiichi Yokogawa,² Keizo Murata,² Noriaki Kimura,³ Haruyoshi Aoki,³ Hiroshi Fukuoka,⁴ Syoji Yamanaka,⁴ Hidekazu Shimotani,⁵ Taishi Takenobu,⁵ Yoshihiro Iwasa,⁵ Takahiko Sasaki,⁶ Norio Kobayashi,⁶ Yuji Miyazaki,⁷ Kazuya Saito,⁸ FangZhun Guo,⁹ Keisuke Kobayashi,⁹ Keiichi Osaka,⁹ Kenichi Kato,¹⁰ Masaki Takata,¹⁰ and Katsumi Tanigaki¹

¹Department of Physics, Graduate School of Science, Tohoku University and CREST-JST, 6-3 Aoba Aramaki Aoba-ku, Sendai, Miyagi 980-8578, Japan

²Department of Physics, Graduate School of Science, Osaka City University, 3-3-138 Sugimoto, Sumiyoshi, Osaka 558-8585, Japan

³Department of Physics, Graduate School of Science, Tohoku University, 6-3 Aoba Aramaki Aoba-ku, Sendai, Miyagi 980-8578, Japan

⁴Department of Applied Chemistry, Faculty of Engineering, Hiroshima University, Higashi-Hiroshima, Hiroshima 739-8527, Japan

⁵Institute for Materials Research, Tohoku University and CREST-JST, 2-1-1 Katahira, Aoba-ku, Sendai 980-8577, Japan

⁶Institute for Materials Research, Tohoku University, 2-1-1 Katahira, Aoba-ku, Sendai 980-8577, Japan

⁷Department of Chemistry, Graduate School of Science, Osaka University, Toyonaka, Osaka 560-0043, Japan

⁸Department of Chemistry, Faculty of Science, Tsukuba University, 1-1-1 Tennoudai, Tsukuba, Ibaraki, Japan

⁹Spring-8, Japan Synchrotron Radiation Research Institute, 1-1-1 Kouto Mikazuki-cho Sayo-gun Hyogo 679-5198, Japan

¹⁰Spring-8, Japan Synchrotron Radiation Research Institute and CREST-JST, 1-1-1 Kouto Mikazuki-cho Sayo-gun Hyogo 679-5198, Japan

(Received 16 February 2005; revised manuscript received 31 May 2005; published 5 October 2005)

Both $\text{Ba}_{24}\text{Si}_{100}$ and $\text{Ba}_{24}\text{Ge}_{100}$ with crystallographically identical structure are found to be superconducting at 1.4 and 0.27 K, respectively. Physical properties of this superconductor $\text{Ba}_{24}\text{Si}_{100}$ are studied by electric transport, specific heat capacity, and magnetic susceptibility measurements. The density of states at the Fermi level $N_{E_F}=0.148$ states eV^{-1} (Si atom)⁻¹ and a distinct jump of C_p at the superconducting transition temperature $\Delta C_p=0.272$ J K^{-1} mol⁻¹ are obtained. An exponential fit of C_p below the superconducting states gives an energy gap $2\Delta=0.423$ meV and shows that this is a superconductor having *s*-wave character or isotropic energy gap. On the basis of our experimental data other important physical parameters are also derived.

DOI: [10.1103/PhysRevB.72.144504](https://doi.org/10.1103/PhysRevB.72.144504)

PACS number(s): 74.70.-b, 74.25.Kc, 74.62.Fj, 79.60.-i

I. INTRODUCTION

Among a variety of clathrates so far reported,¹ the three types as shown in Fig. 1 have intensively been studied. The superconducting silicon network solid was discovered for $\text{Na}_2\text{Ba}_6\text{Si}_{46}$ by Yamanaka's group in 1995,² where Na and Ba atoms are accommodated as endohedral elements inside the silicon polyhedra of Si_{20} and Si_{24} in the type I clathrates. Subsequently, a binary system $\text{Ba}_8\text{Si}_{46}$ was successfully synthesized by the same group using high pressure syntheses.³ Although the attempts to synthesize Ge_{46} compounds with the crystallographically identical structure have been made, no apparent such success has so far been reported.⁴ In contrast to Si_{46} network system (type I clathrate), the superconductivity in the type III clathrates was found in $\text{Ba}_{24}\text{Ge}_{100}$ (Ref. 5) by the group from the MaxPlanck Institute at Dresden.⁶ Although the superconducting transition temperature of T_c at 270 mK found in $\text{Ba}_{24}\text{Ge}_{100}$ was very low, T_c rises up to 3.8 K by applying pressure. This is categorized to one that can be very unique like a certain group of high T_c copper oxide superconductors. $\text{Ba}_{24}\text{Si}_{100}$ with the identical crystal structure to that of $\text{Ba}_{24}\text{Ge}_{100}$ (Refs. 5 and 7) was synthesized under high pressure,⁸ but superconductivity was not reported at that time. However, our recent soft x-ray studies on $\text{Ba}_{24}\text{Si}_{100}$ showed that the density of states at the Fermi level is sufficiently large and the superconductivity has been searched for a high quality sample.

In the present paper, we have shown that the both silicon and germanium clathrates of $\text{Ba}_{24}\text{IV}_{100}$ ($\text{IV}=\text{Si}$ and Ge) with

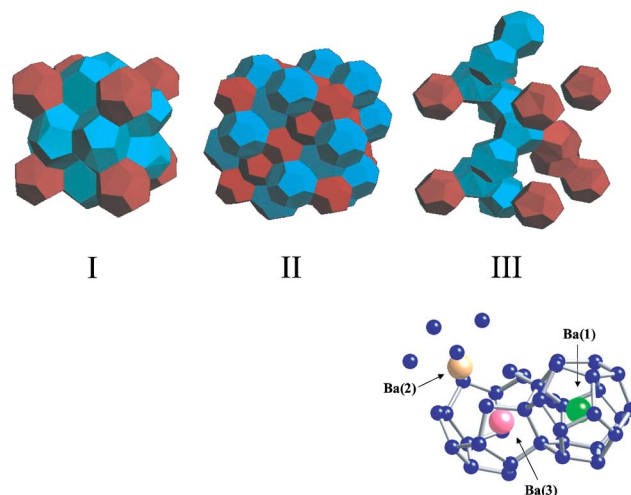


FIG. 1. (Color online) Three types of clathrates classified from type I to III. The type I consists of IV_{20} dodecahedra and IV_{24} tetrakaidecahedra and the type II consists of IV_{20} and IV_{28} hexakaidecahedra. The type III contains closed IV_{20} with helical geometry, pseudocubic cages and open cages. The three kinds of cages are also shown using a ball and stick model.

identical crystal structure are superconductors. Because this a situation that superconductivity occurs both in the Si and Ge polyhedral network solids with crystallographically identical structure after the discovery of superconductivity for these families in 1995, the direct comparison on the fundamental physical parameters between these two superconductors shall give many important insights into the mechanism of superconductivity.^{9–11}

We will exemplify that many physical properties are very much differentiated between Si and Ge polyhedral network solids even if their crystal structures are identical. Especially, it will be highlighted that T_c changes toward a reverse direction between $\text{Ba}_{24}\text{Si}_{100}$ and $\text{Ba}_{24}\text{Ge}_{100}$ upon high pressure. We will discuss the physical properties using the experimental data obtained from specific heat capacity C_p and magnetic susceptibility χ measurements. The evolution of C_p and χ as a function of temperature unambiguously shows that the system can be featured by a large electron-phonon coupling parameter.

II. EXPERIMENT

$\text{Ba}_{24}\text{Si}_{100}$ was synthesized under high pressure according to the previous method.⁸ It is noted that to improve the quality, precise control of both temperature and pressure was needed. Otherwise, superconducting $\text{Ba}_8\text{Si}_{46}$ and BaSi_2 were also produced as contaminants. To obtain x-ray powder diffraction data of good counting statistics with high angular resolution, measurements were carried out at the SPring-8 BL02B2 beam line.¹² For specific heat capacity measurements PPMS (Quantum Design), with a ^3He dilution cryogenerator and a heat capacity cell, was used. The ingot $\text{Ba}_{24}\text{Si}_{100}$ sample weighted by 2.7 mg was put on a platform with four straight wires to measure C_p . In order to figure out the rattling motion, the same measurements were repeated three times at low temperatures below 20 K. Magnetic susceptibilities were measured by a superconducting quantum interference device (SQUID) (Quantum Design MPMS7) system. $\text{Ba}_{24}\text{Si}_{100}$ generally of 7.0 mg was wrapped by a thin plastic film for measurements. Magnetic susceptibilities of the conduction electrons were obtained by subtracting the magnetic moment values measured under 4 T from those under 6 T with a correction of the temperature dependent Curie term.

III. RESULTS AND DISCUSSION

A. Electric transport

The four-probe transport measurement using a ^3He cryostat system showed that $\text{Ba}_{24}\text{Si}_{100}$ enters into a superconducting state at 1.4 K as shown in Fig. 2. No electronic phase transitions were observed until the superconductivity occurs, being different from that of $\text{Ba}_{24}\text{Ge}_{100}$ where a large resistivity upturn is reported at 200 K.¹³ The resistivity at room temperature reduces to one fifth with decreasing temperature. It is very important to emphasize that superconductivity occurs both in Si and Ge networks with the identical crystal

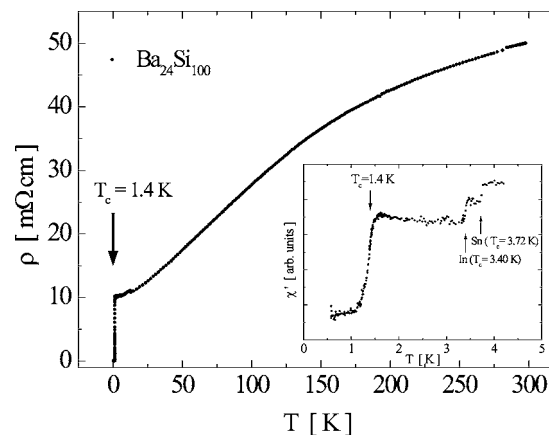


FIG. 2. dc resistivity and ac susceptibility (inset) of $\text{Ba}_{24}\text{Si}_{100}$. The observed values of the ac susceptibilities depend on the geometry of samples and are generally expressed by $\chi_{obs} = -(1/4\pi) \times \{1/(1-(N/4\pi))\}$, where N is the geometry factor. The shape of Sn was spherical ($N=4\pi/3$) while that of $\text{Ba}_{24}\text{Si}_{100}$ and In was spheroidal like. Considering the geometrical correction for such shapes of the measured samples gave almost 100% superconducting fraction.

structure, like diamond Si and Ge, and this is such an example.

We have employed ac susceptibility experiments on this sample in order to confirm whether the observed superconductivity is bulk superconductivity as shown in the inset of Fig. 2. The volume of $\text{Ba}_{24}\text{Si}_{100}$ was estimated to be 1.44 mm^3 using the lattice parameter of $a_0 = 1.407 \text{ nm}$ obtained from x-ray analyses. Although the absolute quantitative analyses need the diamagnetic corrections, the ac susceptibilities calibrated by In (0.73 mm^3) and Sn (0.49 mm^3) as internal standards indicates that $\text{Ba}_{24}\text{Si}_{100}$ is a real bulk superconductor.

It is reported that the T_c observed in $\text{Ba}_{24}\text{Ge}_{100}$ at $\sim 270 \text{ mK}$ was eventually elevated until 3.8 K by applying pressure of 2.7 GPa,⁶ which is generally very unusual in the conventional superconductors. Therefore, we have repeated the experiments. As shown in Fig. 3 (right), the T_c actually rises to 3.2 K under 1.5 GPa. We have also examined how the T_c of $\text{Ba}_{24}\text{Si}_{100}$ changes upon pressure until 1.15 GPa and found that, in contrast to the situation encountered for $\text{Ba}_{24}\text{Ge}_{100}$, the T_c decreases a little as shown in Fig. 3 (left). No structural change has been confirmed in $\text{Ba}_{24}\text{Si}_{100}$ by x-ray diffraction studies under high pressure up to 3 GPa and this is also consistent with the recent high pressure Raman studies.¹⁴

The temperature dependence of the resistivity was not perfectly linear, and small deformation was observed. Since the lattice parameter of the network does not significantly change, such deformation will not be due to the change in the polyhedral framework. The rattling motion of Ba atoms inside the cluster cages may be related to this phenomenon. Actually, as reported in the crystallographically identical $\text{Ba}_{24}\text{Ge}_{100}$ with a larger accommodation space inside the cluster cage, resistivity drastically changes at 200 K from

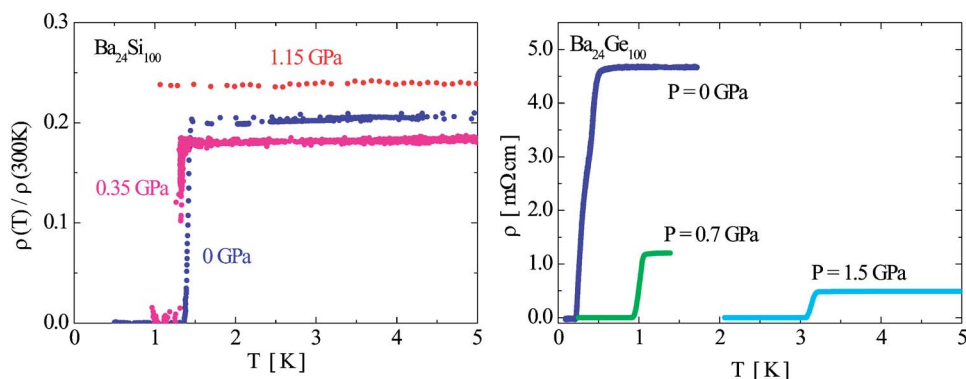


FIG. 3. (Color online) The evolution of resistivities as a function of pressure for $Ba_{24}Si_{100}$ (left) and $Ba_{24}Ge_{100}$ (right).

a high metallic state to a low metallic one.¹³ It should be noted that the resistivity at 300 K of $Ba_{24}Si_{100}$ is 50 m Ω cm and this is larger by 50 times than 1 m Ω cm of $Ba_{24}Ge_{100}$ at 300 K.

B. Magnetic susceptibilities

The magnetic susceptibility of $Ba_{24}Si_{100}$, measured under high magnetic fields using SQUID, was nearly temperature independent and indicates Pauli magnetism. The isolated spin number giving the Curie term appearing at low temperatures was estimated to be 0.063 spins $(Si_{100})^{-1}$ (in the present case, per lattice) and was apparently ascribed to the defects in the crystal. The temperature evolutions of the magnetic susceptibilities after the correction of Curie terms are shown in Fig. 4. The temperature-independent value χ_{const} was $-1.54 \pm 0.12 \times 10^{-3}$ emu $(Si_{100} \text{ mol})^{-1}$ considering the scattering error of the present data. In the same figure, χ_{const} of $Ba_{24}Ge_{100}$ is also displayed at low temperatures and high temperatures straddling the electronic phase transition at 200 K. For extracting the intrinsic Pauli magnetic terms from these data, core diamagnetic susceptibilities were calculated using the values in the literature: -24×10^{-6} for Ba^{2+} , -3.1×10^{-6} for Si, and -7.7×10^{-6} emu mol $^{-1}$ for Ge, giving χ_{core} values of -0.888×10^{-3} for $Ba_{24}Si_{100}$ and -1.35×10^{-3} emu mol $^{-1}$ for $Ba_{24}Ge_{100}$.

Although the concept of diamagnetic susceptibilities produced from the ring current χ_{ring} in the polyhedral cluster solids has not fully been established, such corrections

are known to be needed.⁴ Using the modified Pauling's formula for handling the Larmor diamagnetic susceptibility, $\chi_{ring} = -[ZN_A e^2 / (6mc^2)] \langle r^2 \rangle$ emu mol $^{-1}$,¹⁵ χ_{ring} is evaluated to be -3.28×10^{-3} for $Ba_{24}Si_{100}$ and -3.59×10^{-3} emu mol $^{-1}$ for $Ba_{24}Ge_{100}$. In the formula, Z denotes the number of electrons involved in the cyclic ring current formation, N_A is Avogadro's number, e is the Coulomb charge of an electron, m is the mass of an electron, and c is the speed of light. We used the number of elements constructing polyhedral IV_{20} in the Bravais lattice as Z . These corrections gave the χ_{Pauli} values to be 2.63×10^{-3} for $Ba_{24}Si_{100}$ as well as 2.79×10^{-3} for high- T and 2.10×10^{-3} emu mol $^{-1}$ for low- T phases of $Ba_{24}Ge_{100}$.

Another method of estimation for χ_{Pauli} has been made. Knowing that the ratio of N_{E_F} values in high- T phase to that in low- T phase of $Ba_{24}Ge_{100}$, achieved from soft x-ray photoelectron spectroscopy (XPS),¹⁶ the χ_{Pauli} values can be directly extracted. We have studied the electronic states in the vicinity at the Fermi level using XPS at a high energy radiation facility. As shown in Fig. 5, the density of states at the Fermi level N_{E_F} of $Ba_{24}Ge_{100}$ measured at 300 K reduced at 20 K to a very low value. The change in N_{E_F} observed at 20 K is due to the electronic phase transition, being consistent with the idea of the rattling motion of the endohedral Ba atoms.⁶ These situations are consistent with maximum entropy method (MEM) analyses described later in the present paper.

By optimizing the value of χ_{dia} as an off-set parameter so that the N_{E_F} observed by XPS can be explained, the

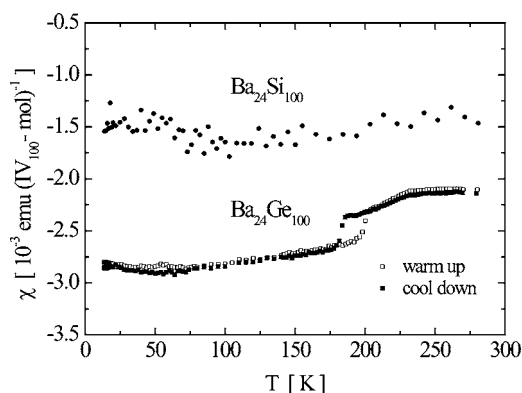


FIG. 4. Magnetic susceptibilities of $Ba_{24}Si_{100}$ and $Ba_{24}Ge_{100}$ after the correction of Curie terms.

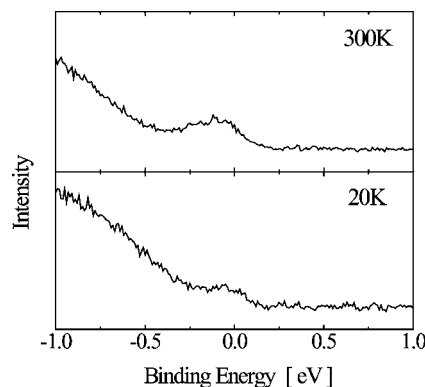


FIG. 5. Electronic states of $Ba_{24}Ge_{100}$ in the vicinity at the Fermi levels measured by soft x-ray spectroscopy at 300 and 20 K. The spectra were normalized by the Ba 5p core spectrum intensity.

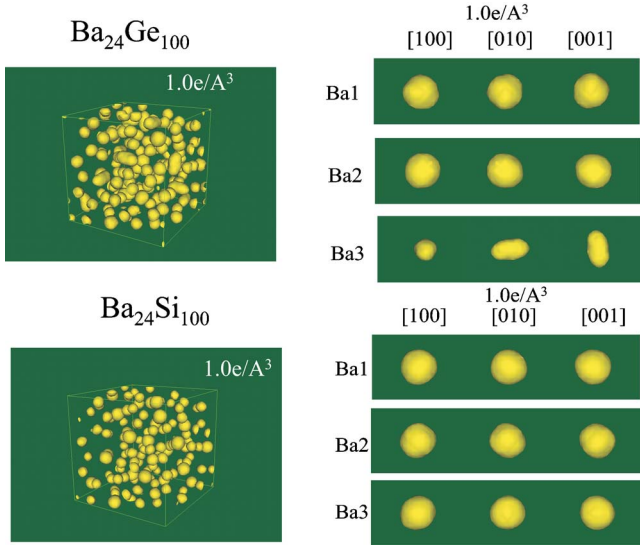


FIG. 6. (Color online) The equi-charge-density surfaces of $\text{Ba}_{24}\text{Si}_{100}$ and $\text{Ba}_{24}\text{Ge}_{100}$ obtained by MEM analyses for high resolution x-ray data at 80 K.

$\chi_{\text{Pauli}} = \chi_{\text{const}} - \chi_{\text{dia}}$ can be evaluated. This method gives more reliable experimental diamagnetic susceptibility χ_{dia} of $\text{Ba}_{24}\text{Ge}_{100}$ to be $-3.11 \times 10^{-3} \text{ emu mol}^{-1}$. When the value of $\text{Ba}_{24}\text{Ge}_{100}$ is scaled to that of $\text{Ba}_{24}\text{Si}_{100}$ using the ratio in χ_{ring} described earlier, χ_{dia} of $\text{Ba}_{24}\text{Si}_{100}$ is estimated to be $-2.50 \times 10^{-3} \text{ emu mol}^{-1}$. As a result, the χ_{Pauli} values can be obtained to be $9.59 \times 10^{-6} \text{ emu (Si mol)}^{-1}$ for $\text{Ba}_{24}\text{Si}_{100}$, $9.65 \times 10^{-6} \text{ emu (Ge mol)}^{-1}$ for the high- T phase, and $2.75 \times 10^{-6} \text{ emu (Ge mol)}^{-1}$ for the low- T phase of $\text{Ba}_{24}\text{Ge}_{100}$. From the relationship $\chi_{\text{Pauli}} = 2\mu_B^2 N_{E_F}$, the N_{E_F} values are determined to be 0.148 states $\text{eV}^{-1} (\text{Si atom})^{-1}$ for $\text{Ba}_{24}\text{Si}_{100}$, 0.149 states $\text{eV}^{-1} (\text{Ge atom})^{-1}$ for the high- T phase, and 0.0427 states $\text{eV}^{-1} (\text{Ge atom})^{-1}$ for the low- T phase of $\text{Ba}_{24}\text{Ge}_{100}$.

There are three kinds of Ba atoms in $\text{Ba}_{24}\text{IV}_{100}$ ($\text{IV} = \text{Si}$ and Ge) from the crystallographical viewpoint as is seen in Fig. 1. In order to see the differences in the rattling motion of Ba between $\text{Ba}_{24}\text{Si}_{100}$ and $\text{Ba}_{24}\text{Ge}_{100}$, a MEM/Rietveld method¹⁷ has been performed. The MEM analysis was carried out with a program ENIGMA¹⁸. Figure 6 showed the equi-charge-density surfaces of these three kinds of Ba atoms at 80 K. Immediately we can recognize that the Ba(3) accommodated in the open cage structure rattles in a very anisotropic fashion, while Ba(1) and Ba(2) atoms do isotropically in the case of the Ge_{100} network. When similar analyses were adopted to the Si_{100} network, such anisotropic electron distributions were not observed even at 80 K. The Ba(3) atoms showing large thermal vibrations at high temperatures will eventually move to a specific trapping site and the equi-charge-density surface will statically become very anisotropic. The reason that such motion was not observed, even in the Ba(3) position in the case of $\text{Ba}_{24}\text{Si}_{100}$, is not apparent at the present stage. It is, however, conceivable that the hybridization of Ba $5d$ and $6s$ orbitals and the $3d$ orbitals of the Ge polyhedra may play an important role in controlling such a rattling motion other than a larger space in the Ge_{100} network than that in Si_{100} one.

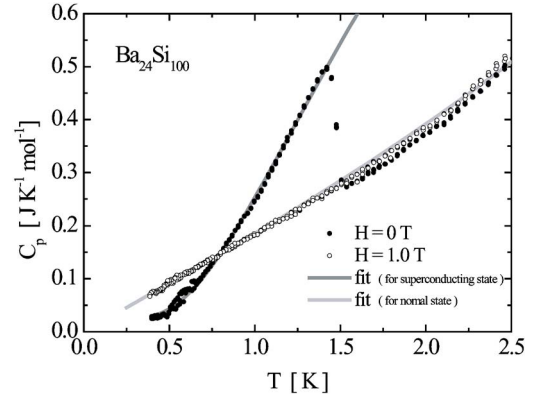


FIG. 7. (Color online) Specific heat capacity C_p of $\text{Ba}_{24}\text{Si}_{100}$. The grey solid lines display fitting curves as explained in the text using $\gamma = 0.182 \text{ J K}^{-2} \text{ mol}^{-1}$, $\Theta_D = 411 \text{ K}$, and $\Theta_E = 46$ and 108 K .

C. Specific heat capacity

Specific heat capacity C_p of $\text{Ba}_{24}\text{Si}_{100}$ is shown in Fig. 7. The specific heat jump at $T_c = 1.4 \text{ K}$ corresponds to the superconducting phase transition observed in electric transport. The evolution of C_p as a function of temperature under the superconducting state can be fitted well using an exponential function of $C_p \sim \exp[-\Delta/k_B T]$ better than T^α function as shown in Fig. 7. This indicates that the superconductivity can be categorized as an s -wave superconductor or a superconductor having an isotropic energy gap. The superconducting energy gap can be estimated to be $2\Delta = 0.423 \text{ meV}$. It is noted here that the C_p data below 8 K scatters to a small extent. Considering the fact that C_p greatly changes at 200 K in $\text{Ba}_{24}\text{Ge}_{100}$ due to the influences of the Ba rattling in the open cage structure,¹³ this phenomenon will be most likely due to the rattled Ba atoms. Although we do not have any exact explanations on this unconventional feature, this was gradually suppressed while the temperature scans were repeated. Therefore, nevertheless of the C_p fluctuations, the Sommerfeld parameter γ was able to be estimated as $0.182 \text{ J K}^{-2} \text{ mol}^{-1}$, from the C_p by applying a standard method of the C_p/T vs T^2 relationship. When $\Delta C_p / \gamma T_c = 1.43$ derived in the weak coupling BCS regime is applied, the γ value was determined to be $0.136 \text{ J K}^{-2} \text{ mol}^{-1}$ as another estimation of γ . These γ values in turn give N_{E_F} to be 0.386 and 0.288 states $\text{eV}^{-1} (\text{Si atom})^{-1}$, respectively.

Owing to the rattling phonons existing at low temperatures, Debye Θ_D and Einstein Θ_E terms may not be obtained with good accuracy directly from the experimental data. Therefore, the Θ_D value was empirically estimated using the Θ_D and Θ_E values of $\text{Ba}_{24}\text{Ge}_{100}$. For this purpose, the following equation can be applied:

$$\begin{aligned} \Theta_D(\text{Ba}_{24}\text{Si}_{100}) &\sim [a_0(\text{Ba}_{24}\text{Ge}_{100})/a_0(\text{Ba}_{24}\text{Si}_{100})] \\ &\quad \times [v(\text{diamond Si})/v(\text{diamond Ge})] \\ &\quad \times \Theta_D(\text{Ba}_{24}\text{Ge}_{100}), \end{aligned}$$

where v is the sound velocity. Because the Ba rattling occurs

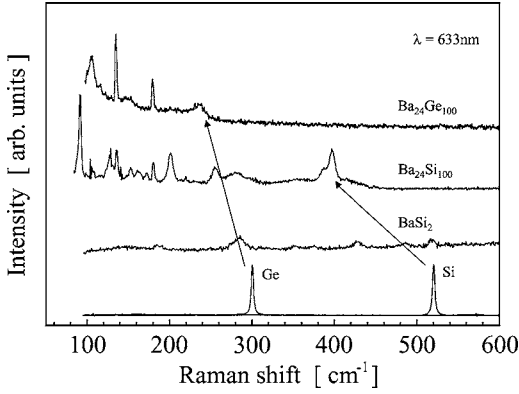


FIG. 8. Raman spectra measured for $\text{Ba}_{24}\text{Si}_{100}$ and $\text{Ba}_{24}\text{Ge}_{100}$ at 300 K. For comparison, the spectra of BaSi_2 , Si, and Ge in the diamond type are displayed. The arrows indicate the corresponding shifts between Si and Ge as described in the text.

at a relatively high temperature of 200 K, hence, it will give little influence on the analyses. From this equation $\Theta_D = 411$ K was estimated for $\text{Ba}_{24}\text{Si}_{100}$ when $v(\text{diamond Si}) = 5.88 \times 10^3$ m s⁻¹, $v(\text{diamond Ge}) = 3.55 \times 10^3$ m s⁻¹ and $\Theta_D = 240$ K for $\text{Ba}_{24}\text{Ge}_{100}$ (Ref. 13) were used. The Einstein Θ_E term was also been empirically scaled by the lattice parameters a_0 between $\text{Ba}_{24}\text{Si}_{100}$ and $\text{Ba}_{24}\text{Ge}_{100}$. The correlation between Θ_E values and lattice parameters can be seen for skutterudite and pyrochlore compounds.¹⁹ When the Θ_E values of 44 and 104 K of $\text{Ba}_{24}\text{Ge}_{100}$ were employed,¹³ $\Theta_E = 46$ and 108 K were obtained using $\Theta_E(\text{Ba}_{24}\text{Si}_{100}) = [a_0(\text{Ba}_{24}\text{Ge}_{100})/a_0(\text{Ba}_{24}\text{Si}_{100})] \times \Theta_E(\text{Ba}_{24}\text{Ge}_{100})$.

Another estimate for the Debye Θ_D and the Einstein Θ_E values could also be possible using the phonon frequency ω data using $\Theta_{D,E}(\text{Ba}_{24}\text{Si}_{100}) = [\omega(\text{Ba}_{24}\text{Si}_{100})/\omega(\text{Ba}_{24}\text{Ge}_{100})] \times \Theta_{D,E}(\text{Ba}_{24}\text{Ge}_{100})$. In order to evaluate the ω values, Raman spectra have been measured and are shown in Fig. 8. Considering the frequency shift observed between 520 cm⁻¹ for ²⁸Si and 300 cm⁻¹ for ⁷⁴Ge, the observed shift of 395 cm⁻¹ for $\text{Ba}_{24}\text{Si}_{100}$ and 235 cm⁻¹ for $\text{Ba}_{24}\text{Ge}_{100}$ can be assigned to the vibrational frequencies of the polyhedral networks. The modes having frequencies below 200 cm⁻¹ observed simultaneously both for $\text{Ba}_{24}\text{Si}_{100}$ and $\text{Ba}_{24}\text{Ge}_{100}$ may be assigned to the Ba modes, but the assignment is very much uncertain at the moment. The frequencies with a less shift ranging from 200 to 300 cm⁻¹ will be ascribed to the Si-Ba and the Ge-Ba vibrational modes. These data are consistent with the recent report.¹³ Using the frequencies of 395 and 235 cm⁻¹ together with $\Theta_D = 240$ K of $\text{Ba}_{24}\text{Ge}_{100}$,^{6,13} Θ_D of $\text{Ba}_{24}\text{Si}_{100}$ was estimated to be 403 K. This is in fairly good agreement with the value estimated using the sound velocity. Due to the experimental inaccuracy in the vibrational modes of the endohedral Ba, Θ_E values were not estimated in the present study.

The Debye and Einstein temperature parameters and the γ estimated earlier from ΔC_p can satisfactorily explain the experimental C_p data of $\text{Ba}_{24}\text{Si}_{100}$, although the influences of the Ba rattling phonons still may scatter the observation for the data.

D. Superconducting parameters of $\text{Ba}_{24}\text{Si}_{100}$

In the concept of the Zintl phase²⁰ for $(\text{Ba}^{2+})_{24}([\text{3b}]\text{Ge}^{1-})_{32}([\text{4b}]\text{Ge}^0)_{68}(16e^-)$,¹³ 16 electrons per Bravais lattice will be considered. Using the lattice constant of 1.407 nm for $\text{Ba}_{24}\text{Si}_{100}$, the electron carrier concentration is 5.75×10^{21} cm⁻³. This is roughly consistent with the carrier concentration n of 2.60×10^{21} cm⁻³ obtained by measurements of the Seebeck coefficient. Applying a three-dimensional electron model to $\text{Ba}_{24}\text{Si}_{100}$ supposing the carrier concentration of 2.60×10^{21} cm⁻³, Fermi wave number k_F of 4.25×10^7 cm⁻¹ is obtained. Using the equations of $\chi_{\text{Pauli}} = 2\mu_B^2[m/(2\pi^2\hbar^2)]k_F$ and $\gamma = [k_B^2 m/(3\hbar^2)]k_F$, $\chi_{\text{Pauli}}^{\text{calc}}$ and γ^{calc} can be estimated to be 5.09×10^{-4} emu mol⁻¹ and 0.0371 J K⁻² mol⁻¹. Although the Ba rattling influences on the specific heat capacity as is pointed out earlier, it is indeed meaningful to have a large enhancement in the experimental γ value ranging from 0.136 to 0.182 J K⁻² mol⁻¹. Actually, the Wilson factor $R_W = (\pi^2 k_B^2 / 3\mu_B^2) [\chi_{\text{Pauli}} / \gamma]$, calculated from the experimental $\chi_{\text{Pauli}}^{\text{exp}}$ and γ^{exp} , is from 0.38 to 0.51 and significantly small. This fact indicates that the system is controlled greatly by electron-phonon interactions rather than electron-electron ones.

In order to explain the T_c of 1.4 K using the McMillan equation, $T_c = [(\Theta_D)/1.45] \exp\{-[1.04(1+\lambda)]/[\lambda - \mu^*(1 + 0.62\lambda)]\}$, $\lambda = 0.399$ is needed for $\Theta_D = 411$ K if one can suppose $\mu^* = 0.1$ (the general value of μ^* ranges from 0.1 to 0.2). Here $\lambda = N_{E_F} V$, V is the electron-phonon coupling parameter, and μ^* is the electron-electron repulsive screening parameter to the Cooper pairing attractive force. If this is the case, a large electron-phonon coupling strength must be constrained in this system considering that the N_{E_F} is small.

From the evolution of specific heat as a function of magnetic field, $[\partial H_{c2}/\partial T]$ can be estimated as a linear plot of H_{c2} vs T_c . Using the WHH equation of $0.69 \times [\partial H_{c2}/\partial T]|_{T=T_c} T_c$, the upper critical field of $H_{c2}(T=0)$ was extrapolated to be 0.24 T. This leads to a Ginzburg-Landau coherence length ξ to be 372 Å using $\xi = [\Phi_0 / [2\pi H_{c2}(T=0)]]^{1/2}$. The mean free path ℓ of conduction electrons can be estimated to be 0.67 Å using $\ell = mv_F / (ne^2\rho)$. Here the resistivity $\rho = 10$ mΩ cm and Fermi velocity $v_F = \hbar k_F / m$ of 4.92×10^7 cm s⁻¹ were employed, and k_F for the carrier concentration was estimated by the Seebeck coefficient. This concludes that $\text{Ba}_{24}\text{Si}_{100}$ is a superconductor classified as a dirty limit of $\ell \ll \xi$.

IV. CONCLUSION

$\text{Ba}_{24}\text{Si}_{100}$ was reported to superconduct like $\text{Ba}_{24}\text{Ge}_{100}$. Physical parameters were obtained for the $\text{Ba}_{24}\text{Si}_{100}$ superconductor from resistivity, specific heat capacity, and ac and dc magnetic susceptibility measurements. The physical parameters derived by these experiments implied that this system can be featured by the extremely strong electron-phonon coupling strength and is a superconductor in the dirty limit. The endohedral Ba atom rattling motion seems to be closely associated with this strong e -ph coupling parameter from the experimental viewpoint and this may open a route for searching exotic materials in the future.

Note Added in Proof. Recently, the superconductivity of $\text{Ba}_{24}\text{Si}_{100}$ was also confirmed²¹.

ACKNOWLEDGMENTS

The synchrotron radiation experiments were performed by the approval of the Japan Synchrotron Radiation Research Institute (JASRI) as a Nanotechnology Support Project. This

work was supported by Creation of Nano Devices and Systems Based on New Physical Phenomena and Functional Principles of CREST of JST. The present work is also partially supported by the Tohoku University 21st century COE program "Particle-Matter Hierarchy" of MEXT, Japan. This work was performed by a Grant-in-Aid from the Ministry of Education, Culture, Sports, Science and Technology of Japan, No. 13304031, 17038801, and 17710088.

-
- ¹Y. Mudryk, P. Rogl, C. Paul, S. Berger, E. Bauer, G. Hilscher, C. Godart, and H. Noël, *J. Phys.: Condens. Matter* **14** 7991 (2002).
²H. Kawaji, H. O. Horie, S. Yamanaka, and M. Ishikawa, *Phys. Rev. Lett.* **74**, 1427 (1995).
³S. Yamanaka, E. Enishi, H. Fukuoka, and M. Yasukawa, *Inorg. Chem.* **39**, 56 (2000).
⁴R. F. W. Herrmann, K. Tanigaki, T. Kawaguchi, S. Kuroshima, and O. Zhou, *Phys. Rev. B* **60**, 13245 (1999).
⁵W. Carrillo-Cabrera, J. Curda, H. G. von Schnering, S. Pachen, and Yu. Grin, *Z. Kristallogr.* **215**, 207 (2000); W. Carrillo-Cabrera, H. Borrmann, S. Paschen, M. Baenitz, F. Steglich, and Y. Grin, *J. Solid State Chem.* **178**, 715 (2005).
⁶F. M. Grosche, H. Q. Yuan, W. Carrillo-Cabrera, S. Paschen, C. Langhammer, F. Kromer, G. Sparn, M. Baenitz, Yu. Grin, and F. Steglich, *Phys. Rev. Lett.* **87**, 247003 (2001).
⁷H. Fukuoka, K. Iwai, S. Yamanaka, H. Abe, K. Yoza, and L. Haming, *J. Solid State Chem.* **151**, 117 (2000).
⁸H. Fukuoka, K. Ueno, and S. Yamanaka, *J. Organomet. Chem.* **611**, 543 (2000).
⁹K. Tanigaki, T. Shimuzu, K. M. Itoh, J. Teraoka, Y. Moritomo, and S. Yamanaka, *Nat. Mater.* **2**, 653 (2003).
¹⁰D. Connetable, V. Timoshevskii, B. Masenelli, J. Beille, J. Marcus, B. Barbara, A. M. Saitta, G. M. Rignanese, P. Mlinon, S. Yamanaka, and X. Blase, *Phys. Rev. Lett.* **91**, 247001 (2003).
¹¹T. Rachi, K. Tanigaki, R. Kumashiro, J. Winter, and H. Kuzmany, *Chem. Phys. Lett.* **409**, 48 (2005).
¹²E. Nishibori, M. Takata, K. Kato, M. Sakata, Y. Kubota, S. Aoyagi, Y. Kuroiwa, M. Yamakata, and N. Ikeda, *Nucl. Instrum. Methods Phys. Res. A* **467–468**, 1045 (2001).
¹³S. Paschen, V. H. Tran, M. Baenitz, W. Carrillo-Cabrera, Y. Grin, and F. Steglich, *Phys. Rev. B* **65**, 134435 (2002).
¹⁴H. Shimizu, T. Kume, T. Kuroda, S. Sasaki, H. Fukuoka, and S. Yamanaka *Phys. Rev. B* **71**, 094108 (2005).
¹⁵R. C. Haddon, L. F. Schneemeyer, J. V. Waszczak, S. H. Glarum, R. Tycko, G. Dabbagh, A. R. Kortan, A. J. Muller, A. M. Muzsca, M. J. Rosseinsky, S. M. Zahurak, A. V. Makhija, F. A. Thiel, K. Raghavachari, E. Cockayne, and V. Elser, *Nature* **350**, 47 (1991).
¹⁶T. Rachi, M. Kitajima, K. Kobayashi, FZ. Guo, T. Nakano, Y. Ikemoto, K. Kobayashi, and K. Tanigaki, *J. Chem. Phys.* **123**, 074503 (2005).
¹⁷M. Takata, E. Nishibori, and M. Sakata, *Z. Kristallogr.* **216** 71 (2001).
¹⁸H. Tanaka, M. Takata, E. Nishibori, K. Kato, T. Iishi, and M. Sakata, *J. Appl. Crystallogr.* **35** 282 (2002).
¹⁹D. Cao, F. Bridges, P. Chesler, S. Bushart, E. D. Bauer, and M. B. Maple, *Phys. Rev. B* **70**, 094109 (2004).
²⁰H. Schäfer, *Annu. Rev. Mater. Sci.* **15**, 1 (1985).
²¹R. Viennois, P. Toulemonde, C. Paulsen, and A. San-Miguel, *J. Phys.: Condens. Matter* **17**, L311 (2005).